Self-diffusivity of liquid silicon measured by pulsed laser melting

P. G. Sanders and M. J. Aziz[a)]
Division of Engineering and Applied Sciences, Harvard University, Cambridge, Massachusetts 02138

(Received 14 May 1999; accepted for publication 7 July 1999)

The silicon liquid self-diffusivity was determined by pulsed laser melting of ^{30}Si ion implanted silicon-on-insulator thin films. Secondary ion mass spectrometry was employed to measure the $^{30}Si^{+}$ concentration-depth profile before and after melting and solidification. Melt depth versus time and total melt duration were monitored by time-resolved lateral electrical conductance and optical reflectance measurements. One-dimensional diffusion simulations were utilized to match the final $^{30}Si^{+}$ experimental concentration spatial profile given the initial concentration profile and the temporal melt-depth profile. The silicon liquid self-diffusivity at the melting point is $(4.0\pm0.5)\times10^{-4}\,cm^2/s$. Calculations of buoyancy and Marangoni convection indicate that convective contamination is unlikely. © *1999 American Institute of Physics.* [S0021-8979(99)02920-5]

INTRODUCTION

Atomic transport properties of liquid silicon are important from both a technological and fundamental perspective. The ubiquitous use of silicon in the semiconductor industry requires many processing steps, some of which involve liquid phase transport, including Czochralski and float-zone crystal growth, as well as pulsed laser-induced thin film crystallization.[1,2] More accurate knowledge of the liquid diffusivity may therefore help in process modeling and control. From a fundamental standpoint, atomistic simulations of silicon systems are common, but there is a paucity of liquid-phase experimental data, the comparison to which provides a critical test of interaction Hamiltonians and methodology. There are currently many reports of the simulated liquid self-diffusivity which are compared only to experimental solute diffusivities due to the absence of an experimental value for the self-diffusivity.

Liquid diffusivity is a particularly challenging property to measure accurately. Two potentially serious problems associated with liquid diffusivity measurements are convective contamination and container wall interactions.[3] The elevated melting point (T_m) and high reactivity of silicon exacerbate both of these problems. Convective contamination generally occurs when there is a temperature gradient in the liquid, creating instabilities that lead to the formation of convective currents. The likelihood of convection is increased at high temperatures and extended times. Although it is exceedingly difficult to completely eliminate convective contamination in terrestrial diffusion measurements, these effects are reduced by fine capillaries that make it difficult to establish convection currents. Although container wall interactions have been ruled out in some diffusion experiments with low T_m materials,[4] the general concern that fine capillaries can introduce problems with wall interactions is appropriate when working with reactive materials at high temperatures.

Liquid diffusivity measurements made by pulsed laser melting can minimize some of the difficulties in making accurate diffusion measurements. The thin film geometry and short melt duration make it virtually impossible to establish convection currents. The planar geometry permits accurate measurement of the submicron diffusion distances resulting from the short melt duration, using techniques such as Rutherford backscattering spectrometry or secondary ion mass spectrometry (SIMS). Because the melted materials are contained by a solid of the same composition, container wall interactions are minimized. Difficulties inherent in this method are the accurate measurement of the temporal melt-depth profile and the liquid temperature. The agreement between time-resolved reflectivity measurements (TRR), SIMS concentration-depth profiles, and heat-flow simulations can minimize uncertainties in both of these quantities.

We are not aware of reported experimental measurements of silicon liquid self-diffusivity. However, there have been measurements of solute diffusivity in silicon, as well as molecular dynamics simulations in which silicon liquid self-diffusivity results are calculated. The chemical similarity of silicon and germanium should lead to comparable magnitudes for silicon liquid self-diffusivity and germanium solute diffusivity in liquid Si. A Ge solute diffusivity of $2.5\times10^{-4}\,cm^2/s$ has been determined in studies of solute partitioning[5] during rapid solidification, in which the solute liquid diffusivity is a fitting parameter in the analysis. Molecular dynamics simulations yield silicon self-diffusivities at T_m in the range of $0.6-2.0\times10^{-4}\,cm^2/s$ (Table I). Simulations using the classical Stillinger–Weber potential have found a weakly activated Arrhenius-type temperature dependence of the silicon liquid self-diffusivity.[11,12] This dependence can be equally well described by a linear temperature dependence over the entire simulated temperature range (1600–1900 K).

EXPERIMENT

The silicon-on-insulator (SOI) samples were fabricated by sequential low-pressure chemical vapor deposition of both SiO_2 and Si films onto (001) Si wafers. In the depth (z) direction, the samples consisted of 355 nm of Si on 255 nm

a)Electronic mail: maziz@harvard.edu

 © 1999 American Institute of Physics

TABLE I. Molecular dynamics simulations.

Method	Si liquid self-diffusivity (10^{-4}cm^2/s)
ab initio pseudopotentials	1.9 (1800 K)[a], 2.3 (1800 K)[b]
Tight-binding	1.1 (1740 K)[c], 1.3 (1780 K)[d], 1.7 (1780 K)[e]
Stillinger–Weber	0.64 (1700 K)[f], 0.65 (1683 K)[g], 0.69 (1691 K)[h]

[a]Reference 6.
[b]Reference 7.
[c]Reference 8.
[d]Reference 9.
[e]Reference 10.
[f]Reference 11.
[g]Reference 12.
[h]Reference 13.

of SiO_2 on Si, as determined from Rutherford backscattering spectrometry (2 MeVHe^+, normal incidence). Photolithography was used to pattern the top Si layer into a serpentine resistor path for use in transient conductance measurements (TCM).[5] Ion implantation of $^{30}Si^+$ at 100 keV to a dose of 4×10^{16} cm^2 produced a $^{30}Si^+$ peak 6 at. % above the natural background of 3.1 at. % at a depth of 150 nm.

The samples were irradiated by a pulsed XeCl excimer laser beam (308 nm, 25 ns FWHM; ~50 ns total duration). After passing through a homogenizer, the laser beam uniformity was ±3% over the 3 mm×3 mm spot. TRR measurements were made using an argon-ion probe laser ($\lambda = 488$ nm) near the Brewster angle. TCM data provided time-resolved melt-depth information, but photoconductivity limited the usefulness of the initial TCM data during the laser pulse. To simplify data interpretation, the ion implantation damage was reduced by first crystallizing each sample with a low-fluence shot (0.3 J/cm^2). The specimens were then melted from 1 to 5 times using a nominal fluence of 0.75 J/cm^2, which typically produced melt durations of 155 ns and melt depths of 180 nm.

The $^{30}Si^+$ depth profiles were determined by SIMS, performed on a Physical Electronics 6650 Quadrupole mass spectrometer using 5 keV O_2^+ ions and monitoring the $^{30}Si^+$, $^{28}Si^+$, and $^{16}O^+$ secondary ions. Secondary ion signals were accepted from the central 5% of the 300 μm craters, with a defocused 700 eV electron beam providing charge compensation. The $^{30}Si^+$ channel was 0.5 a.m.u. wide and the signal was monitored for 5 s per data point, while the $^{28}Si^+$ channel was 0.3 a.m.u. wide and monitored for 1 s per data point. The absolute depth scale was determined by locating the Si/SiO_2 interface using changes in the oxygen signal. The $^{30}Si^+$ concentration calibration was made using the ratio of the $^{30}Si^+$:$^{28}Si^+$ ion yield.

DATA ANALYSIS

The top half of the silicon film was amorphous after $^{30}Si^+$ ion implantation. The initial low-fluence shot resulted in explosive crystallization[14] mediated by a very short-lived melt, yielding a slight change in the $^{30}Si^+$ concentration upon crystallization (Fig. 1). This ''crystallized'' profile was the initial concentration profile used in all diffusion simulations.

One-dimensional heat-flow calculations[15,16] using silicon thermophysical properties[17] were used to simulate the laser melt profiles. During resolidification, the TCM melt profiles agreed well with simulated melt profiles calculated for the same laser fluence (Fig. 2). However, while the laser was firing (the first 50 ns), the TCM signal was dominated by photoconductance. For this reason, simulated melt profiles were used in the diffusion simulations. The simulated melt durations also corresponded well with the FWHM from TRR (Fig. 2). Although the gradually decaying tail of the reflectance trace implies that the crystal–melt interface deviates from planarity, this should not be detrimental because $^{30}Si^+$ does not segregate at the interface. The fluences used in the melt profile calculation were selected by matching the melt durations measured by TRR. The simulated fluence was 0.01–0.02 J/cm^2 less than the experimental fluence, most likely resulting from variations in the sample surface reflectivity from the literature value.

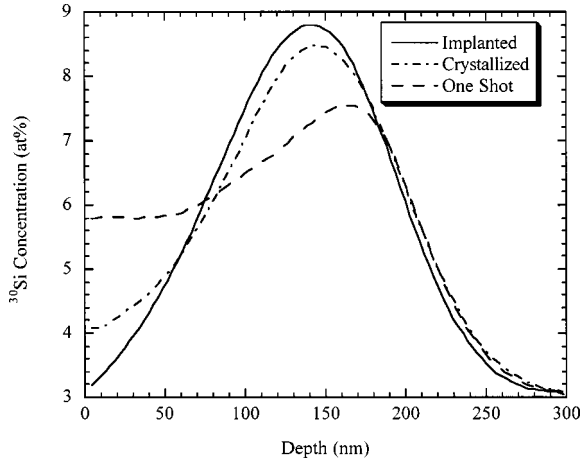

FIG. 1. Concentration profiles of $^{30}Si^+$ from SIMS showing as implanted profile and the changes after a low fluence shot (0.30 J/cm^2) for crystallization and a higher fluence shot (0.75 J/cm^2) typical of those used for the diffusion calculations. The crystallized profile was used as the initial condition for the diffusion calculations.

The simulated silicon melt temporal profile and initial solute concentration-depth profile (after crystallization) were used in solving the one-dimensional diffusion equation[18] to obtain the final solute concentration profile. For samples shot

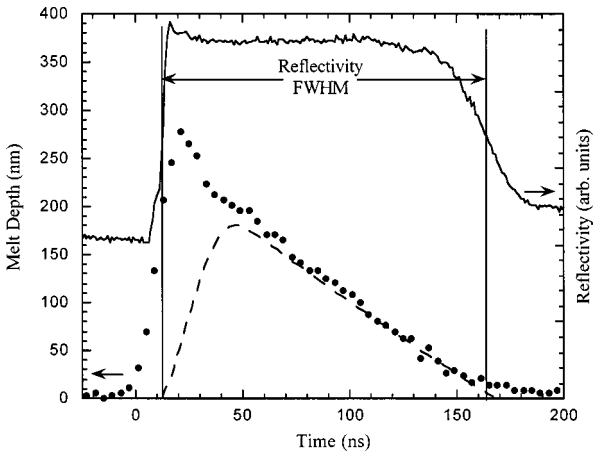

FIG. 2. Comparison of experimental melt profile from transient conductance measurements (circles) with melt profile from heat-flow simulations (dashed line) and the reflectivity trace (solid line). The melt duration of the simulation matches the reflectivity FWHM. Photoconductivity during the laser pulse renders the conductance data useless during the first 50 ns.

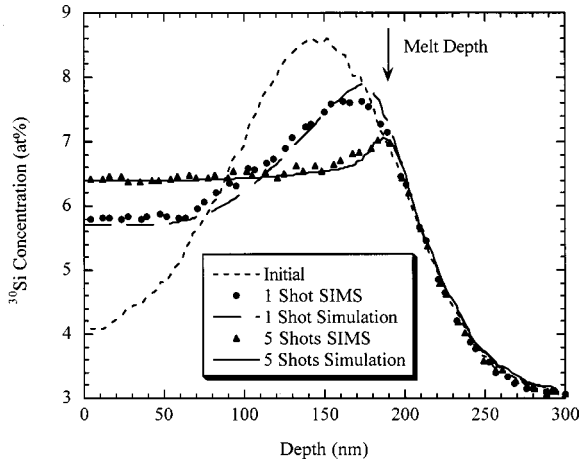

FIG. 3. Agreement between experimental SIMS concentration profile and simulated diffusion profiles for one shot and five shots. The melt depth is shown to be approximately 190 nm.

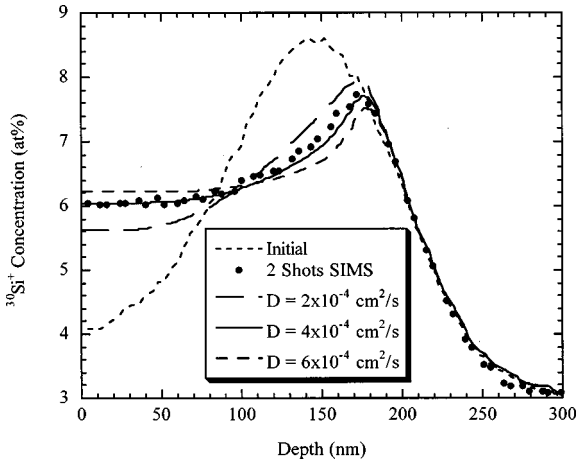

FIG. 4. Comparison between experimental SIMS concentration profile and simulated diffusion profiles after two shots with diffusivities of 2×10^{-4}, 4×10^{-4}, and 6×10^{-4} cm^2/s.

multiple times, the output of the previous simulation was used as the input, and the fluence and diffusivity were kept constant throughout. For each sample, the simulated fluence was varied from 0.74 to 0.76 J/cm^2 and the diffusivity was varied from 2×10^{-4} to 6×10^{-4} cm^2/s to minimize chi-squared between the final calculated diffusion profile and the final measured $^{30}Si^+$ profile. The slight fluence adjustment was needed to match the melt depths observed in the SIMS profiles, as identified by the location of the divergence of the melted and unmelted concentration profiles (Fig. 3). To account for the spatial energy variation of the laser beam, reported diffusion profiles were a Gaussian-weighted average of a suite of diffusion profiles calculated at the best-fit fluence $\pm3\%$ (the measured spatial variation of the laser beam). All concentration profiles were normalized to the initial concentration profile, and chi-squared minimization over only the melt depth was used to select the best-fit liquid diffusivity for each specimen.

RESULTS AND DISCUSSION

The silicon liquid self-diffusivity at the melting point was found to be $(4.0\pm0.3)\times10^{-4}$ cm^2/s. This result is the average and standard error of the four measurements reported in Table II. Additional uncertainties in the melt profile calculation and SIMS calibration increase the standard error to $(4.0\pm0.5)\times10^{-4}$ cm^2/s. In Table II, the average experimental melt duration is the average melt duration per shot determined from reflectivity, whereas the average simulated melt duration is the best-fit melt duration used in the diffusion calculations. The agreement between the SIMS profiles and the diffusion simulations for one and five shots is shown in Fig. 3. An indication of the analysis sensitivity can be obtained from Fig. 4, in which the $^{30}Si^+$ SIMS profile for the sample shot two times is plotted with diffusion simulations at $D=2$, 4, and 6×10^{-4} cm^2/s. Clearly 4×10^{-4} cm^2/s is the best fit of the three.

One important parameter in reporting the diffusivity is the temperature. Heat-flow simulations were done to determine the average liquid temperature during the course of the experiment. For small temperature ranges, the temperature dependence of the diffusivity is expected to be linear. This view is supported by Stillinger–Weber calculations of the diffusivity temperature dependence.[11,12] As shown in Fig. 5, the average liquid temperature is very near T_m. In fact, the simulations indicate that the time-averaged temperature ranges from T_m+3 K at the surface to T_m+12 K near the

TABLE II. $^{30}Si^+$ liquid self-diffusivity measurements.

Number of Shots	Average melt duration (measured) (ns)	Average melt duration (simulated) (ns)	Diffusivity (cm^2/s)
1	168	160	4.3×10^{-4}
2	151	152	3.5×10^{-4}
3	152	156	4.4×10^{-4}
5	162	156	3.7×10^{-4}

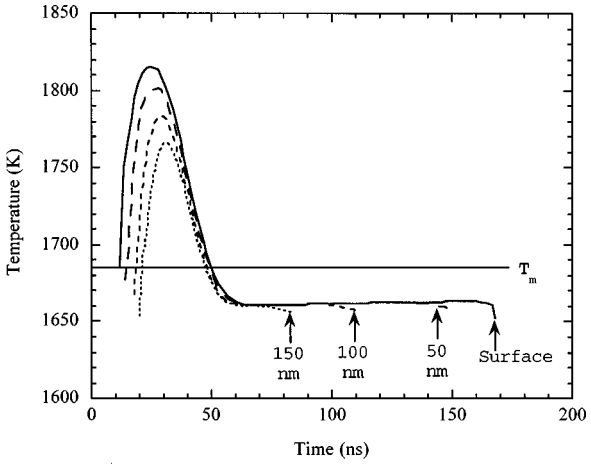

FIG. 5. Liquid temperature temporal profiles at various depths determined by heat-flow calculations. The surface (solid line) melts first and freezes last, while material at 150 nm depth (dotted curve) melts later and freezes earlier. When the solidification front passes a given depth, the corresponding temperature suddenly drops from the essentially steady-state value of 1660 K during solidification (60–170 ns).

full-melt depth. Therefore, the measured diffusivity should correspond to the average melt temperature, which in this case is T_m.

With certain restrictions, it can be shown that the effective liquid diffusivity is equal to the diffusivity at T_m. A flat liquid temperature distribution in z (resulting from, e.g., an infinite liquid thermal conductivity) and a linear melting and freezing velocity response ($v \propto [T - T_m]$ where T is the crystal/melt interface temperature) can be shown to yield a temporal temperature profile at any depth (Fig. 5) for which the integral of the portion of the curve above T_m is equal and opposite to that below T_m. This implies that the average liquid temperature is T_m at all depths. If the temperature dependence of the liquid diffusivity is linear, then the calculated diffusivity is a function of only the average temperature T_m. Any corrections to this model result from deviations from the above assumptions. The assumption most likely to be in error is the lack of a temperature gradient in the liquid during melt-in.

Convective contamination is always an issue in liquid diffusion measurements. Buoyancy-driven convection occurs as a result of temperature gradients within the specimen. Instabilities leading to natural convection[19] can occur if the Rayleigh number $R > 1700$. For the geometry of this experiment, $R = 6 \times 10^{-11}$. Since R has a cubic dependence on the thickness of the liquid layer, the likelihood of buoyancy-driven convection becomes significant only at melt depths >5 mm, which is much greater than the 180 nm melt depths observed in this work.

Marangoni convection results from surface temperature gradients and the temperature dependence of the surface tension. Calculations of surface tension-driven convection using the Stokes solution to a suddenly accelerated flat plate in an infinite liquid[20] and the surface temperature variations identified in the heat-flow simulations indicate that diffusive transport is 2×10^7 times faster than transport in z due to Marangoni convection. This results primarily from the negligible overheating of the liquid but also from the aspect ratio of the specimen, as the velocity of Marangoni-induced currents in z is reduced from the surface radial velocity by the depth-to-width ratio of the melt. Buoyancy- and surface tension-driven convection currents both would tend to flow in the same direction, but the probability of either contributing to mass transport in this experiment is very low.

SUMMARY

The silicon liquid self-diffusivity was determined by pulsed laser melting of $^{30}Si^+$ ion implanted silicon-on-insulator thin films. One-dimensional diffusion simulations were utilized to match the final $^{30}Si^+$ experimental concentration profile given the initial concentration profile and the melt profile. The silicon liquid self-diffusivity at the melting point is $(4.0 \pm 0.5) \times 10^{-4}$ cm^2/s. Calculations of buoyancy and Marangoni convection indicate that convective contamination is unlikely.

ACKNOWLEDGMENTS

This research was sponsored by NASA Grant No. NAG8-1256. The scientific insights and programming expertise of Michael O. Thompson of Cornell University are gratefully acknowledged. The samples were prepared at the Cornell Nanofabrication Facility with the expert assistance of Michael Skvarla. Ion implantation was performed in the Surface Modification and Characterization Research Center at Oak Ridge National Laboratory. SIMS measurements were made by Thomas Mates in the Department of Materials Science and Engineering at the University of California at Santa Barbara. Howard Stone and Thomas Powers are acknowledged for valuable discussions on convection.

[1] R. S. Sposili and J. S. Im, Appl. Phys. A: Mater. Sci. Process. **67**, 273 (1998).
[2] D. Toet, M. O. Thompson, P. M. Smith, and T. W. Sigmon, Appl. Phys. Lett. **74**, 2170 (1999).
[3] T. Iida and R. I. L. Guthrie, *The Physical Properties of Liquid Metals* (Clarendon, Oxford, 1993), p. 199.
[4] L. B. Jalbert, F. Rosenberger, and R. M. Banish, J. Phys.: Condens. Matter **10**, 7113 (1998).
[5] D. P. Brunco, M. O. Thompson, D. E. Hoglund, M. J. Aziz, and H.-J. Gossmann, J. Appl. Phys. **78**, 1575 (1995).
[6] J. R. Chelikowsky, N. Troullier, and N. Binggeli, Phys. Rev. B **49**, 114 (1994).
[7] I. Stich, R. Car, and M. Parrinello, Phys. Rev. B **44**, 4262 (1991).
[8] R. Virkkunen, K. Laasonen, and R. M. Nieminen, J. Phys.: Condens. Matter **3**, 7455 (1991).
[9] C. Z. Wang, C. T. Chan, and K. M. Ho, Phys. Rev. B **45**, 12227 (1992).
[10] G. Servalli and L. Colombo, Europhys. Lett. **22**, 107 (1993).
[11] W. Yu, Z. Q. Wang, and D. Stroud, Phys. Rev. B **54**, 13946 (1996).
[12] K. Kakimoto, J. Appl. Phys. **77**, 4122 (1995).
[13] J. Q. Broughton and X. P. Li, Phys. Rev. B **35**, 9120 (1987).
[14] M. O. Thompson, G. J. Galvin, J. W. Mayer, P. S. Peercy, J. M. Poate, D. C. Jacobson, A. G. Cullis, and N. G. Chew, Phys. Rev. Lett. **52**, 2360 (1984).
[15] M. O. Thompson, Ph.D. thesis, Cornell University, Ithaca, NY, 1984.
[16] P. Baeri and S. U. Campisano, *Laser Annealing of Semiconductors* (Academic, London, 1982), p. 75.
[17] M. J. Aziz, C. W. White, J. Narayan, and B. Stritzker, *Energy Beam-Solid Interactions and Transient Thermal Processing* (Editions de Physique, Paris, 1985), p. 231.
[18] Solution of one-dimensional diffusion equation with moving interface by Crank–Nicholson algorithm, M. O. Thompson (1998).
[19] P. H. Roberts, in *Non-Equilibrium Thermodynamics: Variational Techniques and Stability* (University of Chicago Press, Chicago, 1966), p. 126.
[20] J. P. Longtin, K. Hijikata, and K. Ogawa, Int. J. Heat Mass Transf. **42**, 85 (1999).